ACS APPLIED MATERIALS & INTERFACES

Research Article

www.acsami.org

Stable Organic Field-Effect Transistors for Continuous and Nondestructive Sensing of Chemical and Biologically Relevant Molecules in Aqueous Environment

Minseong Yun, Asha Sharma, Canek Fuentes-Hernandez, Do Kyung Hwang,† Amir Dindar, Sanjeev Singh, Sangmoo Choi, and Bernard Kippelen*

Center for Organic Photonics and Electronics (COPE), School of Electrical and Computer Engineering, Georgia Institute of Technology, Atlanta, Georgia 30332-0250, United States

Supporting Information

ABSTRACT: The use of organic field-effect transistors (OFETs) as sensors in aqueous media has gained increased attention for environmental monitoring and medical diagnostics. However, stable operation of OFETs in aqueous media is particularly challenging because of electrolytic hydrolysis of water, high ionic conduction through the analyte, and irreversible damage of organic semiconductors when exposed to water. To date, OFET sensors have shown the capability of label-free sensing of various chemical/biological species, but they could only be used once because their operational stability and lifetime while operating in aqueous environments has been poor, and their response times typically slow. Here, we report on OFETs with unprecedented water stability. These OFETs are suitable for the implementation of reusable chemical/biological sensors because they primarily respond to charged species diluted in an aqueous media by rapidly shifting their threshold voltage. These OFET sensors present stable current baselines and saturated signals which are ideal for detection of low concentration of small or large molecules that alter the pH of an aqueous environment. The overall response of these OFET sensors paves the way for the development of continuous chemical/biological nondestructive sensor applications in aqueous media.

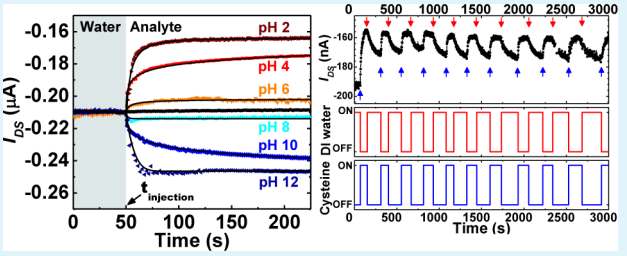

KEYWORDS: *organic field-effect transistor, water-stability, fast chemical detection, reusability*

INTRODUCTION

The remarkable progress in the field of organic electronics has recently raised the interest of the research community toward the development of organic field-effect transistors (OFETs) as read-out devices for various physical,[1,2] chemical, and biological[3] sensing applications. OFETs offer great potential benefits toward the fabrication of a low-cost, printable, flexible, highly sensitive, and selective detection platform.[4,5]

The development of portable sensors that are functional in aqueous media has received attention for applications in environmental monitoring,[6] monitoring of warfare agents,[7] and in situ detection of chemical or biological species for medical diagnostics.[8] If the sensor becomes part of the electronic circuitry in such applications it will eliminate the need for auxiliary detection units. However, the detection of chemical or biological species in aqueous media is highly challenging due to the electrolytic hydrolysis of water and high ionic conduction through the analyte solution at high operating voltages.[9] Several studies on organic electro-chemical transistors (OECTs), used as chemical or biological sensors in aqueous conditions, have emphasized the need for low voltage operation (normally less than 1 V) to avoid these problems.[10] Other FET sensing geometries include ion-sensitive FET (ISFET) wherein sensing occurs on an external reference electrode electrically connected with the FET gate electrode.[11] Sensing in these structures is therefore external to the FET geometry. Insulated gate FETs are another class of chemical sensors wherein the chemical response is driven by a change of the work function of the gate metal in response to an analyte.[12] Their response is slow and, in most cases, does not provide a path toward label-free chemical detection.

OFETs could offer a more favorable platform than OECTs and ISFETs because they can be entirely submerged in aqueous media, since they do not require the use of an electrolyte medium and an external reference electrode: essential components in OECT- and ISFET-based sensors. The key requirement to realize such a reliable OFET-based sensing platform is to achieve stable operation in aqueous environments. Recently, OFETs have been utilized in a broad range of single-use sensing applications including vapor,[13] humidity,[14] pH,[15] glucose,[9,16] biotin,[17] DNA,[15] and drug delivery.[18] However, OFETs operated in humid or aqueous environments show significant degradation of the device's electrical characteristics as a result of the use of high operating voltages and

Received: October 9, 2013
Accepted: January 10, 2014
Published: January 10, 2014

   dx.doi.org/10.1021/am404460j | ACS Appl. Mater. Interfaces 2014, 6, 1616−1622

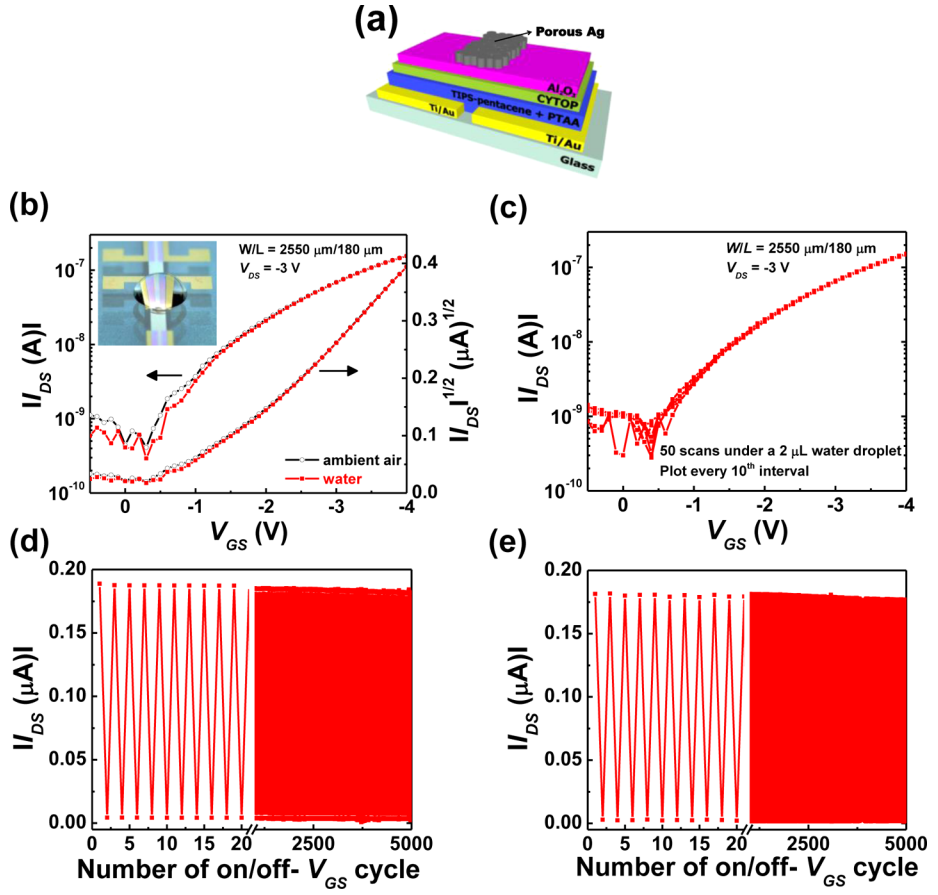

Figure 1. (a) Schematic structure of the top-gate OFET sensors. (b) Transfer characteristics of 25 nm-thick Ag top-gate OFET measured in ambient air and under a 2 μL water droplet placed over the channel, as shown in the inset. (c) Transfer characteristics sequentially recorded up to 50 times under a water droplet. (d) I_{DS} vs V_{GS} (−4 to 4 V) at a V_{DS} (−3 V) measured up to 5000 cycles (1 cycle = 0.1 s) under a water droplet. (e) I_{DS} vs V_{GS} (−3 to 3 V) at a V_{DS} (−2 V) measured up to 5000 cycles (1 cycle = 0.1 s) under flowing water (flow rate of 0.6 mL/min). The initial 20 cycles in parts d and e are expanded for clarity.

electrochemical instability of the organic semiconductor, gate dielectric, and the interfaces formed between the different layers in a transistor.

The operational stability and lifetime of an OFET in water or other aqueous environment has been short because in a bottom-gate geometry, typically used, the organic semiconductor channel is directly exposed to the environment. In this geometry, the organic semiconductor serves a dual function, as an active charge transport layer and as a functional sensing surface.[17,19,20] So far, OFETs have shown either irreversible damage when operated in water or other aqueous solutions, or dramatic changes in their off and leakage currents. For instance, bottom-gate OFETs using the p-channel organic semiconductors 5,5′-bis-(7-dodecyl-9H-fluoren-2-yl)-2,2′-bithiophene and a very thin cross-linked polymer gate dielectric of poly(4-vinylphenol)[15,21] or pentacene-based OFETs passivated with a perfluoro polymer[22] are not irreversibly damaged when operated in aqueous solutions but display dynamic changes in the transistor parameters compared to the ones obtained when operating in air. These dynamic changes arise not only from variations of threshold voltage induced by an analyte but, to a great extent, from variations of the off and leakage currents.[15,17,21,22] These variations of the off and leakage currents are not only undesirable, because they lead to varying baselines and therefore complicate the translation of the changes produced by a given analyte, but they appear systematic when intimate contact between the analyte and the organic semiconductor is needed for sensing to occur, making it very challenging to avoid these parasitic effects while preserving the sensing capabilities of an OFET.[23]

Here, we report on a new sensing geometry based on top-gate OFETs wherein chemical sensing is driven by the diffusion of ionic species. We recently demonstrated that top-gate OFETs based on 6,13-bis(triisopropylsilylethynyl) pentacene (TIPS-pentacene) using a bilayer CYTOP/Al_2O_3 dielectric can display excellent operational and environmental stability.[24] We demonstrate that sensors with this geometry are capable of stable operation in water at low operating voltages; with minimal changes of the OFET characteristics compared with their characteristics in air. In contrast to previous approaches, avoiding intimate contact between the organic semiconductor and the analyte leads to sensors wherein the electronic transduction primarily arises from changes of the threshold voltage. These changes are found to be reversible and reproducible toward various chemical and biologically relevant analytes. This novel OFET sensing geometry could allow the realization of low-cost, portable, and reusable sensors for in situ measurements for the chemical and biological industries.

EXPERIMENTAL SECTION

Fabrication of OFETs. All materials were used as received from Sigma Aldrich unless otherwise stated. The bottom-contact top-gate

dx.doi.org/10.1021/am404460j | ACS Appl. Mater. Interfaces 2014, 6, 1616−1622

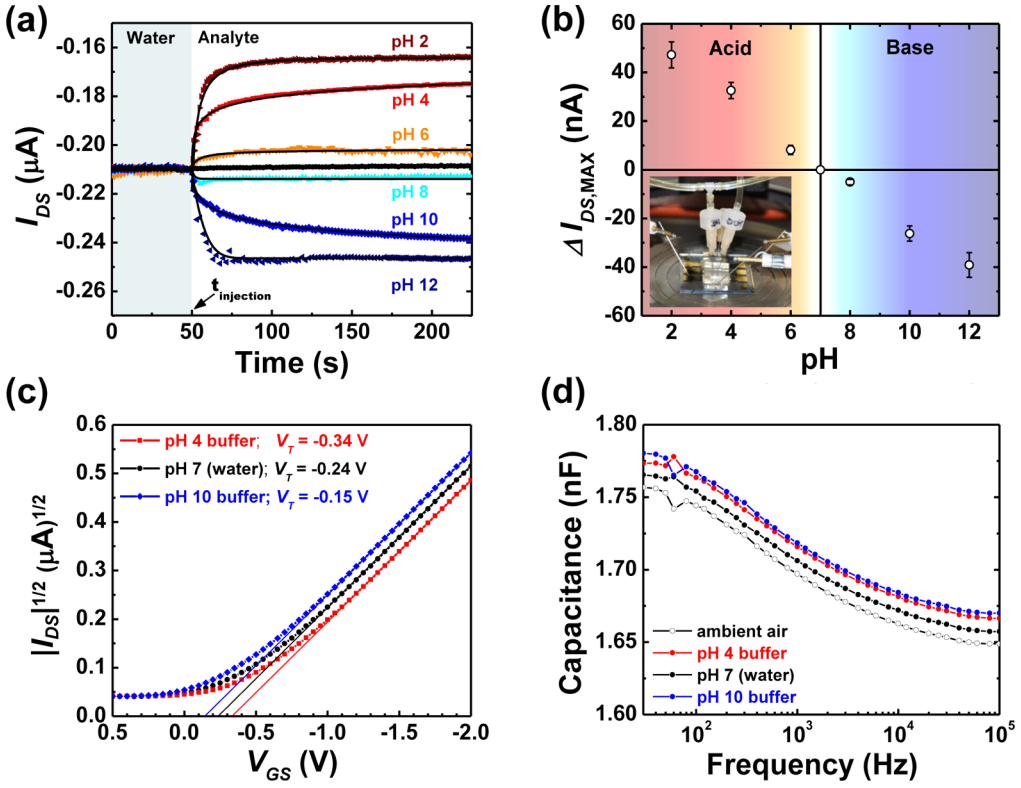

Figure 2. (a) I_{DS} response of 25-nm thick Ag top-gate OFET sensors to pH buffer solutions measured at V_{GS} (−3 V) and V_{DS} (−2 V). The I_{DS} was offset by subtraction of the baseline current after measurement. (b) $\Delta I_{DS,MAX}$ for all pH values analyzed. Inset shows the microfluidic flow cell laminated on the top-gate OFET sensor. The error bars represent the standard deviation calculated over a set of five devices. (c) Transfer characteristics in response to water (pH 7), pH 4, and pH 10 buffer solutions. (d) Frequency-dependent capacitance in air and under a drop of water (pH 7), pH 4, and pH 10 buffer solutions.

OFET sensors were fabricated onto glass substrates (Corning Eagle). Source and drain electrodes were deposited using Ti/Au (6/70 nm) in the Denton e-beam evaporator at a rate of 0.5 Å/s (Ti) and 1 Å/s (Au) under 2 × 10^{-6} Torr at room temperature. The electrode dimensions were defined by using shadow masks with two different sets of channel widths and lengths (3000 μm/150 μm and 2550 μm/180 μm). In order to improve contact between source/drain electrodes and organic semiconductor interface, the substrates were immersed into 10 mM pentafluorobenzenethiol (PFBT) solution in ethanol for 15 min and rinsed by pure ethanol. Then, samples were baked at 60 °C for 5 min. A 1:1 weight ratio of TIPS-pentacene (15 mg) and poly(triarylamine) (PTAA) (15 mg) blend was dissolved in 1,2,3,4-tetrahydronaphtalene anhydrous for a concentration of 30 mg/mL. TIPS-pentacene and PTAA blend was spin-coated at 500 rpm for 10 s at 500 rpm/s acceleration and 2000 rpm for 20 s at 1000 rpm/s acceleration. Then, the samples were immediately annealed at 100 °C for 15 min in hot plate. CYTOP (ASAHI GLASS, CTL-890M) diluted with a solvent (ASAHI GLASS, CT-SOLV180) (1:3.5 volume ratio) was spin-coated on top of the semiconductor layer using 3000 rpm for 60 s with 10000 rpm/s acceleration. Samples were annealed at 100 °C for 10 min in hot plate. All spin-coating and subsequent annealing processes were performed in N_2 filled glovebox. A 50 nm thickness of Al_2O_3 film was grown by Savannah 100 ALD system from Cambridge Nanotech. The film was deposited at 110 °C process temperature using alternating exposures of trimethyl-aluminum ($Al(CH_3)_3$) and water vapor at a deposition rate of approximately 1 Å per cycle. Finally, thermal evaporator was used to deposit different thicknesses of Ag top-gate electrode by using shadow masks for different batch of samples. The base pressures were <5 × 10^{-7} Torr for all depositions at room temperature.

Fabrication of Microfluidic Flow Cell. The poly(dimethlysiloxane) (PDMS) microfluidic flow cell (12 mm × 7 mm × 10 mm) with a flow channel (6 mm ×4 mm ×1 mm) was fabricated by first mixing the base with agent (Gelest OE 41) in a weight ratio of 1:1. The mixed solution was then degassed under vacuum at room temperature. The solution was then gently poured onto the predefined mold (made from thermoplastic) without entrapping any air bubbles. Finally, the predefined mold was transferred to an oven for curing at 80 °C for 1 h under atmospheric pressure. After cooling the mold and peeling the cured microfluidic flow cell off the mold, the flow channel was connected to the outer polyurethane tubing by injecting needle through the flow cell. The outer tip of needle was secured with a Luer Lock coupler. The microfluidic flow cell was attached on the surface of the top-gate OFET, where the direction of liquid flow and OFET channel current was identical. A nonconducting silicon adhesive was used to secure the PDMS flow cell. A liquid flow with 0.6 mL/min flow rate was performed with the help of two variable-flow peristaltic pumps (VWR) equipped with manual flow switch for solution exchanges. One peristaltic pump was used to flow the water and another was used to flow the analyte of interest.

Electrical and Optical Characterizations. All electrical measurements of OFETs, stability, and chemical/biological sensing experiments were carried out using Agilent E5272A source/monitor unit in ambient air. Capacitance-frequency measurements were performed using HP 4284A LCR meter. The capacitance-frequency measurements were performed with the structure of Glass/(Ti/Au)/CYTOP/Al_2O_3/Ag. Droplet of water and pH buffer was placed inside the gate in order to remove potential contributions from the capacitance of droplet outside the gate area. AFM and reflectance data were acquired using Veeco Dimension 3100 AFM and J.A. Woollam M-2000UI ellipsometer, respectively.

RESULTS AND DISCUSSION

Electrical Characteristics of Top-gate OFETs under Water. Figure 1a shows the schematic structure of the bottom-contact top-gate OFET sensors used in the present study.

dx.doi.org/10.1021/am404460j | ACS Appl. Mater. Interfaces 2014, 6, 1616−1622

OFET sensors were fabricated using a blend of TIPS-pentacene and PTAA followed by a bilayer gate dielectric comprised of CYTOP (45 nm) and an atomic layer deposited (ALD) Al_2O_3 (50 nm). OFET operation in water was examined first by placing a 2 μL droplet of deionized (DI) water covering the channel area across the top-gate electrode (as shown in the inset of Figure 1b). As will be explained in the following section, in an OFET sensor with top-gate geometry, the thickness of the top-gate electrode is expected to play an important role toward the sensitivity of the sensor. OFETs were fabricated with 25 nm-, 40 nm-, 70 nm-, and 100 nm-thick Ag top-gate electrodes to first study their stability in water. Ag was chosen because Al or Cu easily oxidizes in water. If the metal is chemically stable in water or other aqueous solutions, then it can be used as top-gate electrode.

Figure S1, Supporting Information, presents a comparison of the transfer characteristics of these OFETs measured in ambient air and in water showing that regardless of the thickness of the gate electrode, the drain-to-source current (I_{DS}) remains unchanged. Figure 1b presents a similar comparison of the transfer characteristics of an OFET having a 25 nm-thick Ag gate electrode in ambient air and in water displaying no significant variations. Mobility (μ) = 0.07 $cm^2/(Vs)$, threshold voltage (V_T) = −0.96 V, and on/off current ratio (I_{on}/I_{off}) = 2×10^3 were measured. As we have reported, the bilayer gate dielectric confers top-gate OFETs not only of excellent environmental stability but also of excellent operational stability.[24] To study the operational stability of OFETs with a 25 nm-thick Ag gate electrode, their transfer characteristics were scanned 50 times while the device was operating in water. Figure 1c displays the unchanged transfer characteristics measured in water; this stability is comparable to that of devices measured in air.[24] No significant changes of the on- and off-currents (I_{on} or I_{off}) (Figure S2, Supporting Information) were found when the operational stability of OFET sensors having Ag gate electrodes with different thicknesses was tested by cycling on- and off-gate-to-source voltage (V_{GS}) with a constant drain-to-source voltage (V_{DS}) for 200 times. For the 25 nm Ag top-gate OFET sensor, the number of V_{GS} cycles was extended to 5000 times. Figure 1d displays the negligible variations of I_{on} and I_{off} found during cycling experiments in static water conditions. Similar experiments were conducted on the 25 nm Ag top-gate OFET sensor during dynamic water flow conditions by laminating a microfluidic flow cell directly onto the surface of the OFET (as shown in the inset of Figure 2b). As shown in the Figure 1e, the OFET sensor also shows stable characteristics up to 5000 cycles during this test. The lack of variation in all the major parameters that characterize the performance of an OFET (μ, V_T, I_{on}/I_{off}, etc.) when operated in air or water is to the best of our knowledge unprecedented.

Sensing Behavior in Top-gate OFET Sensors. Before providing a detailed study of the label-free sensing properties of top-gate OFETs, we must first remember that OFET sensors are charge-sensing devices wherein the I_{DS} for p-type OFETs is described by

$$I_{DS} = \begin{cases} -\frac{W}{L}\mu C_0\left[(V_{GS} - V_T)V_{DS} - \frac{1}{2}V_{DS}^2\right] & (V_{DS} < V_{GS} - V_T) \\ -\frac{W}{L}\mu C_0(V_{GS} - V_T)^2 & (V_{DS} > V_{GS} - V_T) \end{cases} \quad (1)$$

where W is the channel width, L is the channel length, and C_0 is the gate dielectric capacitance density, respectively. For an analyte to be detected, it must induce a change of I_{DS} by a concurrent or individual change on the values of μ, V_T, or C_0. As shown by eq 1, in the saturation regime ($V_{DS} > V_{GS} - V_T$), a sensing mechanism inducing changes of V_T is preferred because I_{DS} follows a quadratic dependence on this parameter, in contrast with the linear dependence on μ or C_0. Although changes of μ and C_0 could arise from the interaction of the semiconductor and gate dielectric with neutral analytes (i.e., by the creation of traps in the semiconductor layer or by a change of density in the gate dielectric), changes of V_T necessarily arise through the presence of charged or polar species. In the proposed structure, chemically or biologically active interlayers can be used to coat the metal-oxide gate dielectric layer or potentially a perforated or porous metallic gate. These layers should display strong binding affinity to the analyte of interest and the binding mechanism would preferably lead to a large change of the electrostatic potential of that layer (i.e., through the formation of ionic or hydrogen bonds).

In bottom-gate OFET sensors, diffusion of an analyte through the semiconductor grain boundary leads to charge trapping or doping/dedoping of the organic semiconductor.[15] Even in materials where the value of μ remains relatively constant, the interaction between the analyte and the organic semiconductor results not only in changes of V_T but also in a severe increase of I_{off}. Avoiding direct contact between the analyte and the organic semiconductor is therefore critical to avoid this parasitic effect.

In contrast, in top-gate OFET sensor geometry, the analyte is less likely to reach the organic semiconductor layer during detection. Instead, the analyte diffuses into the gate dielectric or the metal/dielectric interface to produce changes of V_T and/or C_0. Diffused charged species will ideally have a stronger impact on V_T rather than on C_0. Changes in V_T are preferred because they are sensitive to the polarity (sign) of the diffused charge species and can produce quadratic changes of I_{DS}. In top-gate OFETs, the value of V_T will effectively shift as diffused charged species screen the gate potential, V_{GS}, and create an effective gate voltage (V_{eff}) given by[25]

$$V_{eff} = V_{GS} \pm q\Delta\varphi \quad (2)$$

where $\Delta\varphi$ is the electrostatic potential induced by diffused analytes such as ions, dipoles, etc., and q is the elementary charge. When eq 2 is inserted into eq 1 and terms regrouped, this effective gate potential will produce an apparent shift of V_T equal to $\Delta V_T = \mp q\Delta\varphi$. Note that regardless of the type of semiconducting channel V_T shifts in a direction that is opposite to the sign of the charged species in the analyte. This is, for p-channel OFETs, diffused positive charge species will produce a negative shift of V_T, which in turn will increase the value of $I_{DS}(V_{GS})$. Note that since $I_{DS}(V_{GS})$ is negative for p-channel OFETs, an increase of its value is reflected as a reduction of its absolute magnitude. Conversely, diffused negative charge will produce a positive shift of V_T, which in turn will decrease the value of $I_{DS}(V_{GS})$. For n-channel OFETs, diffused positive charge species will also produce a negative shift of V_T that will increase the value of $I_{DS}(V_{GS})$; in contrast with p-channel OFETs, this will be reflected in an increased absolute magnitude of $I_{DS}(V_{GS})$. Consequently, diffused negative charge species will produce a positive shift of V_T, which in turn will decrease the value of $I_{DS}(V_{GS})$. Hence, in a top-gate OFET sensor, where chemical interactions between the analyte and the semiconductor are prevented, label-free sensing is ultimately pH detection.

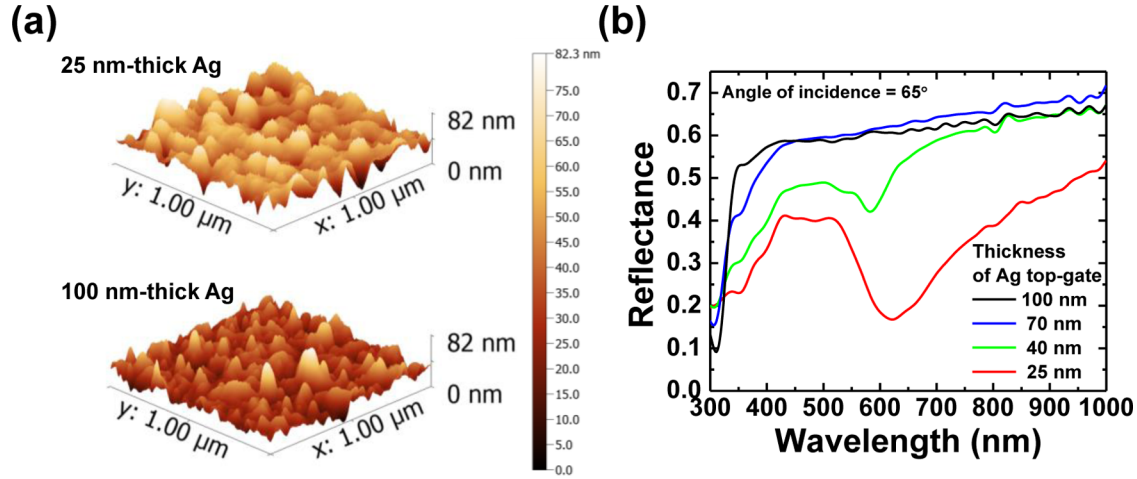

Figure 3. (a) AFM images of 25 nm- and 100 nm-thick Ag electrodes. (b) Reflectance of Ag electrodes with different thicknesses at an angle of incidence of 65°.

With this in mind, the fundamental sensing properties of top-gate OFET sensors were studied using buffer solutions with different pH values (2 to 12) as analytes. Buffer solutions provide the easiest way to systematically study the effects that charged species, namely H^+ and OH^-, have on the response of an OFET sensor. I_{DS} was continuously recorded in flowing water and analyte conditions to conduct these studies. A flow cell system, placed on top of the gate electrode was used to allow control over the flow of aqueous solutions, as shown in the inset of Figure 2b. Prior to insertion of the analyte solution, I_{DS} was monitored for about 50 s at constant V_{DS} and V_{GS} in flowing water to establish a baseline.

OFETs with 100 nm-thick Ag top-gates were found to display very small and slow changes of I_{DS} in response to the pH buffer solutions (Figure S3, Supporting Information). In contrast, OFETs with 25 nm-thick Ag top-gates displayed fast and significant changes of I_{DS} that correlated well with the pH of the buffer solutions, as shown in Figure 2a. For acidic buffer solutions, having pH values below 7, the I_{DS} rapidly increases, yielding a net positive change $\Delta I_{DS}(225\ s) \equiv I_{DS}(225\ s) - I_{DS}(50\ s)$ due to diffused $[H^+]$ ions. Conversely, diffused $[OH^-]$ ions caused an immediate decrease of I_{DS} (net negative change) when a basic buffer solution, having pH values higher than 7, was applied to the gate. Furthermore, as shown in Figure S4, Supporting Information, I_{DS} remains unchanged to water and to a pH 7 buffer. Figure S5, Supporting Information, demonstrates that a similar behavior is observed for n-channel OFET sensor based on bis(thienyl)tetrazine-bridged naphthalene diimide (NDI-BTTZ-NDI), this is, I_{DS} increases in response to acids and decreases in response to basis.

As shown in Figure 2a, the temporal evolution of $I_{DS}(t)$ is described by stretched exponential relation of the form: $I_{DS}(t) = I_{DS}(t \leq 50\ s)[1 \pm \exp(-\{t/\tau\}^{\beta})]^2$ where the positive sign corresponds to basic analytes and the negative sign to acidic ones. Note that the correspondence of pH with the sign in this equation is independent of the type of semiconductor channel used. Stretched exponential behavior has been correlated with the relaxation of a disordered system through dispersive diffusion. Here, it is unclear what underlying processes lead to the stretched exponential behavior, particularly since no systematic variation of β or τ was found when fitting experimental data and since the temporal evolution of sensor response to pH values of 4 and 10 is significantly different from that found in response to other pH values analyzed. However, in all cases, the initial response rate, $\partial I_{DS}/\partial t$, is around 5 nA/s, and with exception of the response to buffers with pH values of 4 and 10, saturation is achieved within 25 s of the analyte being injected. Figure 2b displays $\Delta I_{DS}(225\ s)$ for all pH values analyzed. The amplitude of $\Delta I_{DS}(225\ s)$ for basic solutions was found to be consistently smaller than the one found for acidic solutions with equivalent ionic concentrations, this is, for pH 12 and 2, 4, and 10 or 6 and 8. When the normalized responses $(|\Delta I_{DS}(t)|/\langle I_{DS}\rangle(t \leq 50\ s))$ to all pH values are compared side-by-side, as shown in Figure S6, Supporting Inforamtion, it becomes apparent that discrepancies between basic and acidic analytes with equivalent ionic concentrations, arise from a secondary process that starts 5 to 15 s after a basic analyte has been injected. Otherwise, at early stages of the response $\Delta I_{DS}(t)$ is the same for analytes with equivalent ionic concentrations. The fast response and appearance of clearly saturated signals in top-gate OFET sensors are a significant improvement over bottom-gate OFET sensors reported in the literature. Figure S7, Supporting Information, demonstrates that flexible top-gate OFET sensors display a similar response toward a pH buffer analyte when bended or flat.

As discussed in the previous section, in a top-gate OFET sensor $\Delta I_{DS}(t)$ arises either from changes of V_T and/or C_0. The transfer characteristics and capacitance of a 25 nm-thick top-gate OFET sensor were measured in water (pH 7), pH 4, and pH 10 buffer solutions. Figure 2c and 2d displays the results of these measurements and confirms that $\Delta I_{DS}(t)$ arise primarily from changes of V_T rather than from changes of capacitance. This is because, as expected from eqs 1 and 2, V_T undergoes a negative shift when the OFET sensor is exposed to acidic solutions and a positive shift when exposed to basic solutions. At the same time, the frequency-dependent capacitance data suggests changes smaller than 1% in the direct current (dc) capacitance in the presence of acidic or basic analytes; a hypothesis further supported by the constant slopes displayed by the transfer characteristics of the OFET sensors under various analytes (Figure 2c). Note that the in the presence of water the capacitance only varies by 0.8% with respect to air.

The increased sensitivity of top-gate OFET sensors with 25 nm-thick gate electrodes compared to those having 100 nm-thick gate electrodes is explained as follows. For sensing to occur, the analyte must diffuse into the OFET structure.

dx.doi.org/10.1021/am404460j | ACS Appl. Mater. Interfaces 2014, 6, 1616−1622

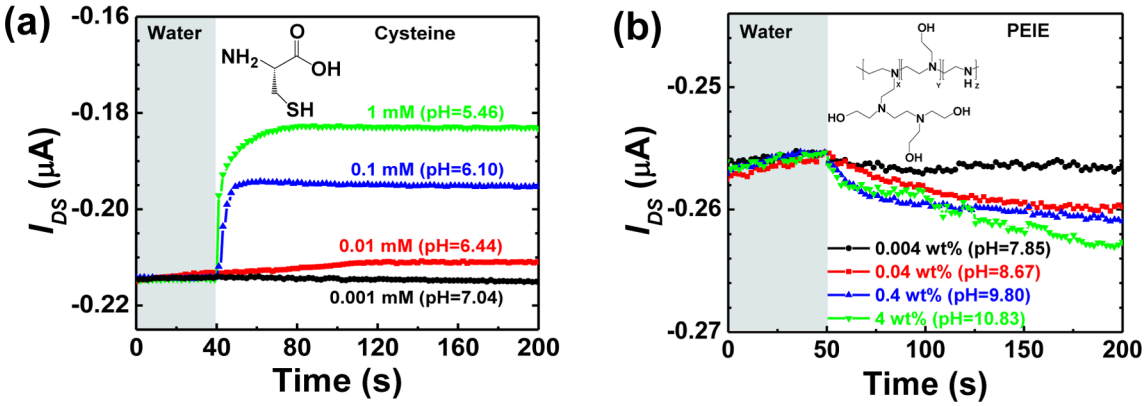

Figure 4. I_{DS} response of 25 nm-thick Ag top-gate OFET sensor to different analytes: (a) cysteine, V_{GS} (−2 V) and V_{DS} (−1 V); (b) PEIE, V_{GS} (−2 V) and V_{DS} (−1 V).

Diffusion can occur "horizontally", by the sides of the gate electrode, or "vertically", through the gate electrode. Given the big differences in length scales, vertical diffusion is believed to be much more efficient than horizontal diffusion. Hence, the sensitivity of a top-gate OFET sensor will heavily depend on the thickness and porosity of the gate electrode. As we have shown, neither thickness nor porosity will affect its operational stability. The porosity, and consequently the roughness, is expected to be higher in a 25 nm-thick Ag gate electrode than in a 100 nm-thick Ag gate electrode. This is because the surface energy mismatch between a metal and a dielectric, forces a metal film to grow in the Volmer−Weber mode during its deposition, first forming nanometer-scale islands that grow to form interconnected networks and only form continuous films after sufficient material has been deposited.[26] Atomic force microscopy (AFM) images shown in Figure 3a, reveal a much larger root-mean squared (RMS) roughness value of 11 nm in 25 nm-thick Ag electrodes than the value of 4 nm found in 100 nm-thick Ag electrodes. To further correlate the increased surface roughness with the morphology of the Ag layer, the reflectance of Ag electrodes with different thicknesses was measured at an angle of incidence of 65°. Figure 3b shows the signature of a clear surface plasmon resonance in the visible range in Ag electrodes with thicknesses less than 40 nm. In 25 nm-thick Ag films, this resonance is spectrally broader and red-shifted compared to the one observed in 40 nm-thick Ag electrodes. A red shift indicates that a larger portion of the surface polariton interacts with the Al_2O_3 layer, as supposed to air, and a spectrally broader signature indicates larger size heterogeneity of metallic domain sizes; expected of metallic films that are more porous and closer to the percolation threshold. Hence, the increased sensitivity of OFET sensors having 25 nm-thick Ag gate electrodes can be explained by the increased porosity of their electrodes and consequently an increased facility for charged species to diffuse into the OFET structure. Hence, further improvements in detector sensitivity and response time could be achieved by engineering the nanoporosity of this electrode.

Detection of Chemical and Biologically Relevant Species using Top-gate OFET Sensors. The ability of a top-gate OFET sensor to perform label-free detection of traces of chemical and/or biological species depends upon the ability of these molecules to alter the pH of their aqueous solvent, their ability to diffuse into the OFET sensor, and any chemical interactions that may exist between the analyte and the metal gate or metal-oxide gate dielectric. As a first example, we explored the sensing of cysteine, an α-amino acid that represents a biologically relevant species of significant interest for the health industry. When cysteine is mixed with water, it creates an acidic solution with a pH that varies from 5.46 at a concentration of 1 mM to around 7.04 at 0.001 mM. Figure 4a displays the response of the OFET sensor to cysteine solutions varying within aforementioned range. As expected for acidic solutions, the sensor presents a positive $\Delta I_{DS}(t)$ with a fast initial response and signals that saturate within the first 30 s of being exposed to the cysteine solution, for concentrations larger than 0.1 mM (pH > 6) and within around 80 s for the 0.01 mM concentration. As would be expected from the neutral pH, a negligible signal was found for the 0.001 mM concentration. Because the diffusion process is expected to be dependent on the size of the molecules we want to detect, we explored sensing of high molecular-weight water-soluble cationic polymers containing simple aliphatic amine groups, such as polyethylenimine (PEIE). Naturally derived cationic polymers are itself of great biological interest as nonviral gene delivery systems. When dissolved in water, cationic polymers create basic solutions. As shown in the Figure 4b, the sensor presents a negative $\Delta I_{DS}(t)$ with a slower response and smaller amplitude than the one observed for basic buffer solutions. Hence, suggesting that the ease of molecules to diffuse into the OFET sensor plays a role in the response of the sensor and will have to be facilitated in future OFET sensors by, for instance, engineering the porosity of the top-gate electrode.

Finally, top-gate OFET sensors pave the way for the development of reusable real-time nondestructive sensors. Figure 5 displays the real-time monitoring of continuous cycles of sensor exposure to a 0.1 mM cysteine solution in water followed by pristine water, over a period of 3000 s. From this data, it is clear that while the detection of cysteine is fast, its out-diffusion during the water cycle is slower and may be incomplete. This leads to a reduced contrast of $\Delta I_{DS}(t)$ from around 50 nA in the first cycle, to around 20 nA during subsequent cycles. Optimization of the duty cycle, to extend the time the sensor sees water, and reversing the polarity of the gate, to assist in the out-diffusion of charged species, are expected to improve the magnitude of $|\Delta I_{DS}(t)|$ during continuous operation. However, the present results already demonstrate the remarkably good reproducibility of the sensor signal toward the label-free continuous detection of an analyte.

dx.doi.org/10.1021/am404460j | ACS Appl. Mater. Interfaces 2014, 6, 1616−1622

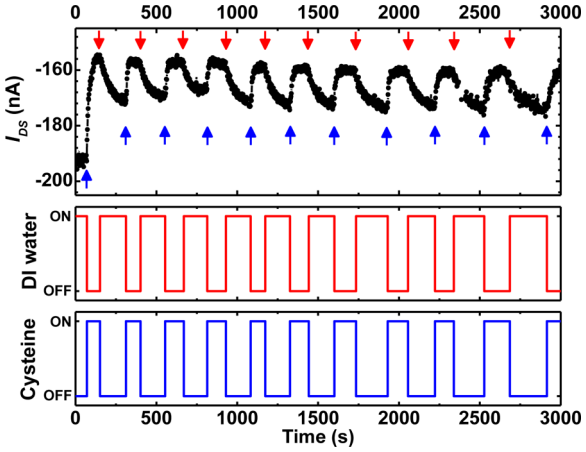

Figure 5. I_{DS} response of 25 nm-thick Ag top-gate OFET sensor to continuous cycling of a 0.1 mM cysteine solution and water, measured at V_{GS} (−3 V) and V_{DS} (−2 V). The blue arrow indicates start of cysteine flow and red arrow indicates start of water flow.

CONCLUSIONS

We demonstrated top-gate OFET sensors with unprecedented stability and response in aqueous environments. These sensors lead to the label-free detection of chemical or biologically relevant species provided that these species have the ability to alter the pH of an aqueous solvent. Shifts of the threshold voltage of the OFET sensor are primarily responsible for the ability of these sensors to detect charged species in a solvent. The direction of these shifts correlates inversely with the sign of the charged species in the solvent. Engineering of the porosity of the metal-gate electrode should lead to improvements in the sensitivity and response time of these top-gate OFET sensors without sacrificing their stable performance in aqueous media. Top-gate OFET sensors pave the way toward the development of real-time reusable OFET sensors. Although the selectivity and sensitivity of these sensors may lag behind those of less stable OFET sensors reported in the literature, chemical approaches to functionalize the gate dielectric or top-gate could further improve the selectivity and sensitivity of our sensors but may preclude their reusability if the analytes bind too strongly with the functional layers. The proposed top-gate OFET sensors are expected to bring sensing applications of chemical and biological molecules in aqueous media one step closer to commercial realization.

ASSOCIATED CONTENT

Supporting Information

Transfer and cycling characteristics measured under water, I_{DS} response of 100 nm-thick Ag top-gate OFET sensors, I_{DS} response of 25 nm-thick Ag top-gate n-channel OFET sensors, and I_{DS} response of Ag top-gate OFET sensor on PES substrate. This material is available free of charge via the Internet at http://pubs.acs.org.

AUTHOR INFORMATION

Corresponding Author

*E-mail: kippelen@ece.gatech.edu.

Present Address

[†]Interface Control Research Center, Future Convergence Research Division, Korea Institute of Science and Technology (KIST), Seoul 136-791 (South Korea)

Notes

The authors declare the following competing financial interest(s): B.K. served as consultant to Solvay and received compensation for these services. This study could affect his personal financial status. The terms of this arrangement have been reviewed and approved by Georgia Tech in accordance with its conflict of interest policies.

ACKNOWLEDGMENTS

This material is based upon work supported by Solvay S.A. and the Science and Technology Center Program of the National Science Foundation (DMR-0120967).

REFERENCES

(1) Sekitani, T.; Yokota, T.; Zschieschang, U.; Klauk, H.; Bauer, S.; Takeuchi, K.; Takamiya, M.; Sakurai, T.; Someya, T. *Science* **2009**, *326*, 1516−1519.
(2) Sekitani, T.; Takamiya, M.; Noguchi, Y.; Nakano, S.; Kato, Y.; Sakurai, T.; Someya, T. *Nat. Mater.* **2007**, *6*, 413−417.
(3) Lin, P.; Yan, F. *Adv. Mater.* **2012**, *24*, 34−51.
(4) Torsi, L.; Lovinger, A. J.; Crone, B.; Someya, T.; Dodabalapur, A.; Katz, H. E.; Gelperin, A. *J. Phys. Chem. B* **2002**, *106*, 12563−12568.
(5) Someya, T.; Dodabalapur, A.; Huang, J.; See, K. C.; Katz, H. E. *Adv. Mater.* **2010**, *22*, 3799−3811.
(6) Johnson, K. S.; Needoba, J. A.; Riser, S. C.; Showers, W. J. *Chem. Rev.* **2007**, *107*, 623−640.
(7) Voiculescu, I.; McGill, R. A.; Zaghloul, M. E.; Mott, D.; Stepnowski, J.; Stepnowski, S.; Summers, H.; Nguyen, V.; Ross, S.; Walsh, K.; Martin, M. *IEEE Sens. J.* **2006**, *6*, 1094−1104.
(8) Owens, R. M.; Malliaras, G. G. *MRS Bull.* **2010**, *35*, 449−456.
(9) Someya, T.; Dodabalapur, A.; Gelperin, A.; Katz, H. E.; Bao, Z. *Langmuir* **2002**, *18*, 5299−5302.
(10) Kergoat, L.; Piro, B.; Berggren, M.; Horowitz, G.; Pham, M. C. *Anal. Bioanal. Chem.* **2012**, *402*, 1813−1826.
(11) Bartic, C.; Borghs, G. *Anal. Bioanal. Chem.* **2006**, *384*, 354−365.
(12) Janata, J.; Josowicz, M. *Nat. Mater.* **2002**, *2*, 19−24.
(13) Crone, B.; Dodabalapur, A.; Gelperin, A.; Torsi, L.; Katz, H. E.; Lovinger, A. J.; Bao, Z. *Appl. Phys. Lett.* **2001**, *78*, 2229−2231.
(14) Li, D. W.; Borkent, E. J.; Nortrup, R.; Moon, H.; Katz, H.; Bao, Z. N. *Appl. Phys. Lett.* **2005**, *86*, 042105−3.
(15) Roberts, M. E.; Mannsfeld, S. C.; Queralto, N.; Reese, C.; Locklin, J.; Knoll, W.; Bao, Z. *Proc. Natl. Acad. Sci. U.S.A.* **2008**, *105*, 12134−12139.
(16) Liu, J.; Agarwal, M.; Varahramyan, K. *Sens. Actuators, B* **2008**, *135*, 195−199.
(17) Magliulo, M.; Mallardi, A.; Gristina, R.; Ridi, F.; Sebbatini, L.; Cioffi, N.; Palazzo, G.; Torsi, L. *Anal. Chem.* **2013**, *85*, 3849−3857.
(18) Angione, M. D.; Cotrone, S.; Magliulo, M.; Mallardi, A.; Altamura, D.; Giannini, C.; Cioffi, N.; Sabbatini, L.; Fratini, E.; Baglioni, P.; Scamarcio, G.; Palazzo, G.; Torsi, L. *Proc. Natl. Acad. Sci. U.S.A.* **2012**, *109*, 6429−6434.
(19) Torsi, L.; Farinola, G. M.; Marinelli, F.; Tanese, M. C.; Omar, O. H.; Valli, L.; Babudri, F.; Palmisano, F.; Zambonin, P. G.; Naso, F. *Nat. Mater.* **2008**, *7*, 412−417.
(20) Duarte, D.; Dodabalapur, A. *J. Appl. Phys.* **2012**, *111*, 044509−7.
(21) Roberts, M. E.; Mannsfeld, S. C. B.; Stoltenberg, R. M.; Bao, Z. *Org. Electron.* **2009**, *10*, 377−383.
(22) Khan, H. U.; Jang, J.; Kim, J.-J.; Knoll, W. *Biosens. Bioelectron.* **2011**, *26*, 4217−4221.
(23) Spijkman, M.-J.; Brondijk, J. J.; Geuns, T. C. T.; Smits, E. C. P.; Cramer, T.; Zerbetto, F.; Stoliar, P.; Biscarini, F.; Blom, P. W. M.; de Leeuw, D. M. *Adv. Funct. Mater.* **2010**, *20*, 898−905.
(24) Hwang, D. K.; Fuentes-Hernandez, C.; Kim, J.; Potscavage, W. J.; Kim, S.-J.; Kippelen, B. *Adv. Mater.* **2011**, *23*, 1293−1298.
(25) Possanner, S. K.; Zojer, K.; Pacher, P.; Zojer, E.; Schuerrer, F. *Adv. Funct. Mater.* **2009**, *19*, 958−967.
(26) Wang, Z.; Cai, X.; Chen, Q.; Li, L. *Vacuum* **2006**, *80*, 438−443.